JACC: CARDIOVASCULAR IMAGING
VOL. 8, NO. 9, 2015

ISSN 1936-878X/$36.00
PUBLISHED BY ELSEVIER INC.
http://dx.doi.org/10.1016/j.jcmg.2015.08.001

Noninvasive Imaging of Flow and Vascular Function in Disease of the Aorta

Matthew C. Whitlock, MD,* W. Gregory Hundley, MD*†

ABSTRACT

With advancements in technology and a better understanding of human cardiovascular physiology, research as well as clinical care can go beyond dimensional anatomy offered by traditional imaging and investigate aortic functional properties and the impact disease has on this function. Linking the knowledge of the histopathological changes with the alterations in aortic function observed on noninvasive imaging results in a better understanding of disease pathophysiology. Translating this to clinical medicine, these noninvasive imaging assessments of aortic function are proving to be able to diagnose disease, better predict risk, and assess response to therapies. This review is designed to summarize the various hemodynamic measures that can characterize the aorta, the various noninvasive techniques, and applications for various disease states. (J Am Coll Cardiol Img 2015;8:1094–106) © 2015 by the American College of Cardiology Foundation.

Recognized as a conduit for distributing blood, abnormalities of the functional properties of the aorta are increasingly realized as important contributors to cardiovascular (CV) disease. This review is designed to summarize the various functional properties of the aorta, noninvasive imaging methodologies used to assess these properties, and abnormalities of these properties that contribute to CV disease.

The aorta performs several important functions. First, the aorta transmits and distributes blood from the heart to medium-sized conduits that supply the periphery. Second, the aorta acts as an expandable reservoir that buffers the pulsatile force from left ventricular contraction (1). The Windkessel principle, first outlined in the late 1800s, models the aorta as an elastic reservoir absorbing the systolic blood flow from left ventricular contraction and then releasing this blood by elastic recoil during diastole providing more constant (rather than pulsatile) blood flow to the periphery (2). Finally, a healthy aorta limits the augmentation phenomenon from the reflective pressure wavefronts that return toward the heart from the medium sized conduits that supply the periphery (3). As the pressure wavefront from ventricular contraction propagates down the vasculature tree, reflections of these wavefronts return from the periphery and amplify the systolic pressure within the aorta that thereby increases left ventricular afterload. This mechanical interplay between the left ventricle and the arterial tree is termed ventricular arterial coupling with the aorta playing an integral role in this relationship (4). In healthy normals, under a wide range of vascular loading conditions, the aorta allows for optimized work efficiency in conjunction with the left ventricle (5); however, alterations in the vessel wall and loss of these properties that occur with aging and disease processes can reduce circulatory efficiency (6).

Optimal function of the aorta is related to the structure and composition of 3 regions of the wall of the aorta (**Figure 1**): the intima, media, and adventitia (7). The intima comprises the endothelium, the endothelial glycocalyx, which is a network of glycosaminoglycans bordering the vessel lumen (8), and the endothelial space, which contains collagen and sparse smooth muscle cells (7). With aging, flow-mediated vasoreactivity is diminished (9) and the intima exhibits increased collagen deposition and disoriented vascular smooth muscle cells (10).

The media, the thickest layer of the aorta and separated from the intima by the internal elastic

From the *Department of Internal Medicine, Section on Cardiovascular Medicine, Wake Forest School of Medicine, Winston-Salem, North Carolina; and the †Department of Radiological Sciences, Wake Forest School of Medicine, Winston-Salem, North Carolina. The research was supported in part by grants from the National Institutes of Health (R01HL076438, R33CA121296, R01CA167821, T32HL091824, and R01HL118740) and from the Susan G. Komen Foundation (BTR0707769). All authors have reported that they have no relationships relevant to the contents of this paper to disclose.

Manuscript received April 2, 2015; revised manuscript received August 3, 2015, accepted August 6, 2015.

lamina contains layers of overlapping sheets of the extracellular matrix proteins elastin and collagen and vascular smooth muscle cells (11). Elastin is capable of stretching over 300% of its original length but fractures at relatively low levels of stress (12). Collagen is less pliable but is capable of handling much higher stress loads and thus provides significant strength to the aorta (12). In the proximal thoracic aorta, an elevated elastin to collagen ratio heightens vascular compliance; whereas distally in the abdominal aorta, collagen and smooth muscle predominate leading to a stiffer conduit (13,14). With aging, the percent of collagen increases in the media (15) and cross linking and abnormal breakdown of the proteins due to mechanical fracturing as well as oxidation and nonenzymatic glycation occurs (6,16).

The adventitia is the outermost layer and is composed mainly of collagen, fibroblasts, and fibrocytes (7). The adventitia reinforces aortic wall strength (to limit excessive aortic distension) and also anchors the vessel to the surrounding tissues. The adventitia also contains the vasa vasorum, the supporting blood supply to the cells of the aorta. With aging, increased collagen accumulation from fibroblasts have been seen in animal studies contributing to stiffening (17).

At a macroscopic anatomic level, the aorta diameter grows in relationship to increasing body surface area during the time from infant to young adulthood (18). With further aging, the arterial wall thickens, predominantly in the intima and the aorta dilates, greater in the ascending aorta as compared to the abdominal aorta (19).

VASCULAR BIOMECHANICS

Both simple and complex measures quantify the biomechanical functional properties of the aorta (**Table 1**). As shown in **Figure 2**, the simplest measures include blood velocity and flow (which couples velocity with vessel area to measure the volume of fluid traversing a defined point per unit time).

Additional simple measures include stress, strain, and Young's modulus, which relates the two. Stress is defined as the force per unit area applied to an object, and within a blood vessel specific types of stress are defined by the direction of force include radial, circumferential, and longitudinal stress (**Figure 2**). For example, arterial pressure exerts outward force on the vessel wall resulting in circumferential stress. Strain, ε, quantifies the deformational response of the tissue to a force:

Equation 1: $$\varepsilon = \frac{L - L_o}{L_o}$$

where L is the final dimension after applied stress and L_o is the starting dimension. The relationship between stress and strain in a material is defined by the constant, Young's modulus, which is the ratio of stress to strain. A very rigid material has a very high Young's modulus (i.e., with stress, the aortic tissue deforms very little).

When fluid such as blood travels within a structure, there is also wall shear stress, which represents frictional force of the fluid parallel to the flow of the fluid. In other words, blood flowing along the vessel wall creates a "drag" force in the direction of blood flow on the endothelial cells (**Figure 2**).

Building on these basic equations, more complex measures of aortic function have been derived. Arterial compliance represents the change in the diameter of a vessel divided by the change in the distending pressure within the vessel. This is essentially the reciprocal of Young's modulus in a cylinder. Arterial distensibility is similar to compliance but is normalized for the size of the vessel. Aortic distensibility is the degree to which the aorta can expand such that a stiff vessel has low distensibility. Using 2-dimensional (2D) imaging techniques, distensibility can be expressed as follows (20):

Equation 2: $$Distensibility\left(\frac{1}{mmHg \times 10^3}\right) = \frac{(SA - DA)}{DA \times (SBP - DBP)}$$

where SA is the maximal systolic area, DA is the minimal diastolic area, SBP is systolic blood pressure millimeters of mercury (mm Hg), and DBP is diastolic blood pressure. Due to the peripheral amplification phenomenon, brachial blood pressures do not always accurately reflect central blood pressures, particularly in younger subjects and thus, should not be used as a surrogate (21). Noninvasively, several methods to estimate central blood pressure have been developed using pressure waveforms taken from carotid, brachial or radial arteries and calibrated to cuff pressures. The strengths and limitations of these techniques are reviewed elsewhere (22).

Pulse wave velocity (PWV) is another measure of aortic stiffness and is related to the Young's modulus by the Moens-Korteweg equation (1):

Equation 3: $$PWV = \sqrt{\frac{E \times h}{2 \times r \times \rho}}$$

where E is circumferential Young's modulus, h is vessel wall thickness, r is luminal radius, and ρ is

ABBREVIATIONS AND ACRONYMS

2D = 2-dimensional
3D = 3-dimensional
4D = 4-dimensional
cfPWV = carotid-femoral pulse wave velocity
CKD = chronic kidney disease
CT = computed tomography
CV = cardiovascular
MRI = magnetic resonance imaging
PC = phase contrast
PWV = pulse wave velocity
TTE = transthoracic echocardiography

FIGURE 1 Cross-Sectional Diagram of the Aortic Vessel With the Components of the 3 Layers in a Healthy Young Individual (20 Years of Age) and in an Elderly Individual (70 Years of Age) Demonstrating the Effects of Arterial Aging

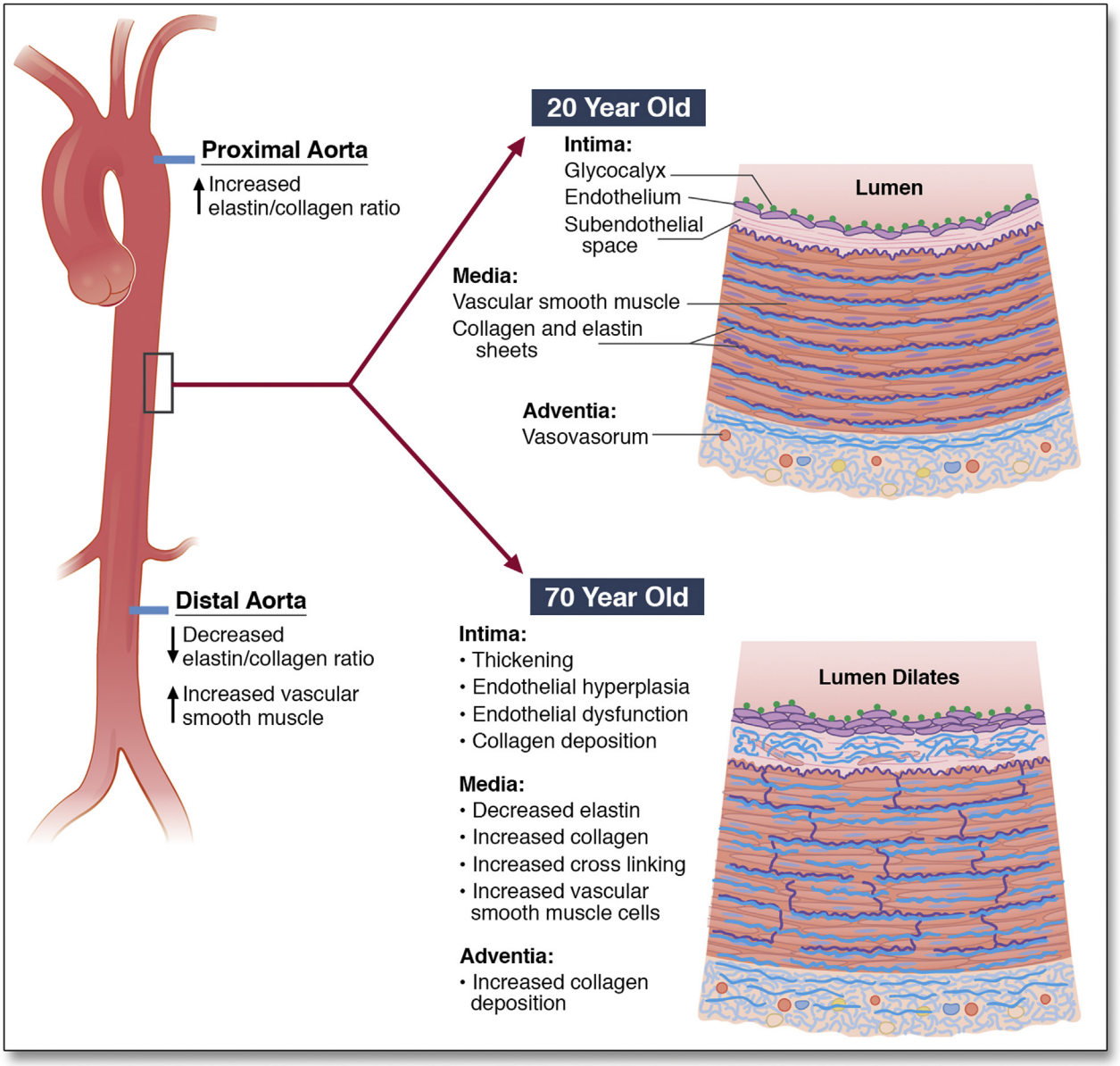

With aging, the endothelium experiences thickening with hyperplasia and collagen deposition. The media has increased disorganized smooth muscle cells, increased collagen, and increased elastin fracturing and cross linking. The adventitia demonstrates increased collagen deposition.

density of blood. Recall earlier that Young's modulus is the ratio of stress to strain in a material; thus, a rigid material (high Young's modulus) will result in a high PWV, all else equal. Descriptively, PWV represents the measure of how fast the systolic pulse from a volume of blood being ejected from the left ventricle travels down the aorta. In general, a stiffer more rigid vessel transmits the pulse faster (higher PWV). PWV and distensibility are inversely related to one another by the Bramwell-Hill equation (23):

Equation 4: $$PWV = \frac{3.57}{\sqrt{Distensibility}}$$

TABLE 1 Noninvasive Imaging Modalities Useful in the Aorta and Subsequent Measurements of Aortic Flow and Function Capable by Each Modality

Modality	Measurement
Echocardiography	Velocity Flow Tissue strain Pulse wave velocity Distensibility Pressure gradient
Cardiovascular CT	Distensibility Tissue strain
Cardiovascular MR	Velocity Flow Flow visualization and pattern Flow displacement Pulse wave velocity Distensibility Pressure gradient and maps Wall shear stress

CT = computed tomography; MR = magnetic resonance.

when units of mm Hg and meters per second are used. In clinical practice, PWV is calculated by recording (commonly using transducers located at the carotid artery and femoral artery, hence carotid-femoral PWV [cfPWV]) 2 locations separated by a known distance. By recording at the same time or by triggering relative to the electrocardiogram, the transducers determine the difference in the arrival time of the systolic wavefront at each location. The distance, in meters, along the aorta between the 2 transducers is divided by the difference in arrival time, in seconds, yielding a velocity in meters per second.

Equation 5:

$$PWV(m/s) = \frac{Distance}{difference\ in\ pulse\ arrival\ times}$$

Accurate PWV determinations rely on several factors. First, one must accurately measure the distance along the blood vessel that the pulse wave has traversed. Body surface estimations can be affected by body habitus, such as obesity, or by tortuosity of the blood vessels that is unknown when simply estimating the path by looking at the body surface. Second, the fact that blood is flowing in opposite directions in the carotid and femoral arteries needs to be taken into account either by measurement technique or converted via formula (24). Finally, cfPWV is considered a global measure of aortic stiffness; however, the ascending aorta from the root to the takeoff of the right brachiocephalic is not included due to measuring from the peripheral sites of the carotid and femoral arteries. This area may represent a clinically important source of aortic stiffening in certain disease states.

Pressure gradients within the aorta can be estimated from Doppler echocardiography and phase contrast (PC) magnetic resonance imaging (MRI) by utilizing Bernoulli's principle. With several

FIGURE 2 Cross-Sectional Diagram of an Aorta Demonstrating the Biomechanical Measures of Velocity, Flow, and Stress

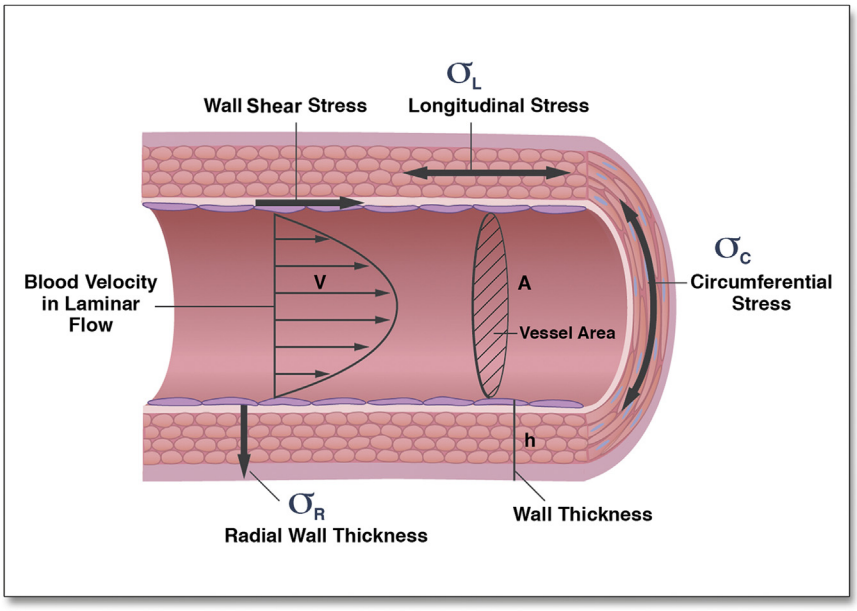

JACC: CARDIOVASCULAR IMAGING, VOL. 8, NO. 9, 2015
SEPTEMBER 2015:1094–106

CENTRAL ILLUSTRATION **Examples of Different Imaging Modalities Used to Assess Aorta Flow and Function**

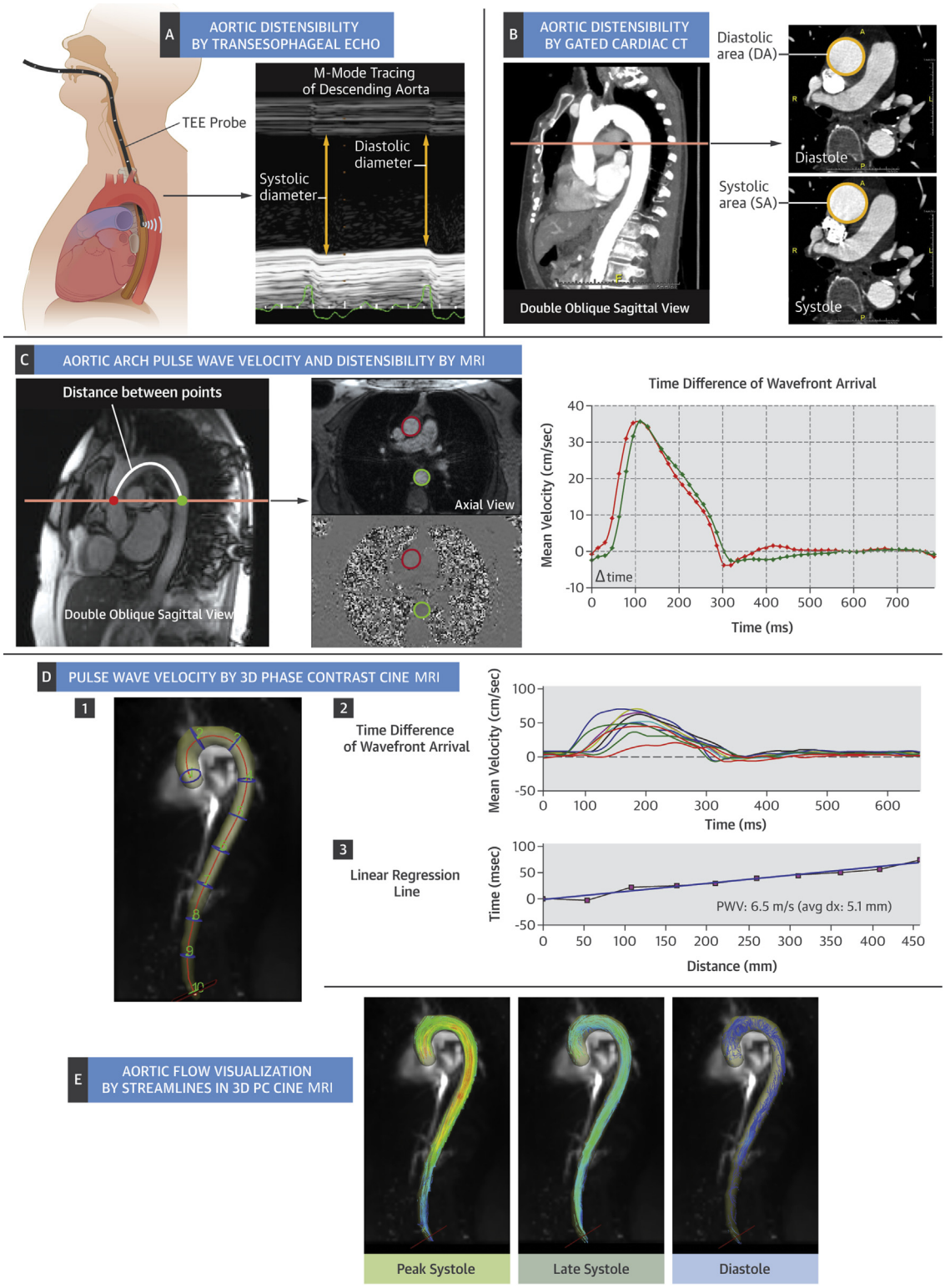

Whitlock, M.C. et al. J Am Coll Cardiol Img. 2015; 8(9):1094–106.

Continued on the next page

assumptions, the equation relating velocity at 2 locations (v_b, v_a) to pressure is the modified Bernoulli's equation (25):

Equation 6: $$Pressure\ Difference = 4\left(v_b^2 - v_a^2\right)$$

when using the units of mm Hg and meters per second.

Newer imaging technologies have provided additional visualization capabilities, including 3-dimensional (3D) flow changes with time. This has led to additional measures including blood flow eccentricity or displacement (26), pressure gradients (27), and blood turbulence quantification (28). These are further discussed in the MRI section.

IMAGING MODALITIES

ECHOCARDIOGRAPHY. Echocardiography uses ultrasound waves and their differential reflection from body tissues to create 2D and 3D images of CV structures (29) as well as quantifying velocity of structures by employing the Doppler effect (30). With known blood velocity over a period of time (velocity time integral) and vessel area, the volume of blood per heart beat traversing the vessel can be quantified (30). Additional computation allows for the assessment of strain within the wall of the aorta using tissue Doppler (31) or speckle tracking technology (32). Focusing on the individual components of the arterial wall, the longitudinal strain and wall shear stress within the 3 layers of the aortic wall can also be evaluated with echo (33). Additionally, Doppler-derived velocity measurements allow one to calculate pressure differences within the aorta using modified Bernoulli's equation (Equation 6) (34).

Distensibility assessed by transthoracic echocardiography (TTE) is typically measured in the ascending aorta just above the aortic valve using the M-mode aortic diameter at end-systole and end-diastole. This technique has shown excellent correlation with invasive measurements (35) and can be used to measure other aortic regions including the abdominal aorta (36). Transesophageal echocardiography can be used in a similar fashion to TTE using M-mode tracings (37) (**Central Illustration**, panel A) or 2D cross-sectional cine images (38) with the advantage of measuring multiple levels of the descending aorta as to reduce the risk of sample bias at a single location.

Three-dimensional transesophageal echocardiography (39) and TTE (40) can also be used to measure distensibility of the aorta. The advantage of these techniques relates to the acquisition of a large 3D volume data set of the aorta from which post-exam processing allows for measuring multiple regions of interest.

Pulse wave velocity can be measured using ultrasound Doppler in similar fashion to the pressure transducer technique described previously. By placing the ultrasound probe at the carotid artery and the femoral artery, the Doppler-derived arrival time difference of the velocity waveforms can be calculated. In comparison with applanation tonometry derived cfPWV, correlation is excellent (41,42).

CARDIAC COMPUTED TOMOGRAPHY. Gated to the cardiac cycle, cardiac computed tomography (CT) is able to produce tomographic images of the aorta at different phases in the cardiac cycle (43). Using this technology, distensibility of the aorta can be assessed (**Central Illustration**, panel B). In a similar fashion to

CENTRAL ILLUSTRATION Continued

(A) Transesophageal echocardiography measuring aortic distensibility using a M-mode tracing of the descending aorta. The systolic and diastolic diameters are measured from the tracing and used with the central blood pressure to calculate distensibility. **(B)** Gated cardiac computed tomography assessing aortic distensibility. A sagittal image of the aorta arch displays the location of the axial plane gated at systole and diastole. The systolic and diastolic areas of the ascending aorta are used with the central blood pressure to calculate distensibility. **(C)** Two-dimensional phase contrast cine magnetic resonance imaging (MRI) measuring pulse wave velocity. A sagittal image of the aorta arch displays the location of the axial plane and is used to calculate the vessel centerline distance between the ascending and descending aorta. Through plane phase contrast and magnitude, images in the axial plane are segmented for the ascending and descending aorta, and velocity versus time flow curves are generated (**red** is from the ascending aorta, **blue** is from the descending). The time difference between the arrival of 2 waveforms is determined. Pulse wave velocity is calculated by dividing the distance by the arrival time difference. Distensibility of the ascending and descending aorta can be calculated from the change in diastolic and systolic areas from the magnitude images and the central blood pressure. **(D)** MRI using 4D flow assess multiplane pulse wave velocity: 1) 10 analysis planes placed equidistantly along the 3-dimensional segmented aorta containing 3-direction velocity information; 2) 10 through-plane velocity versus time waveforms derived from the 10 analysis planes, and the time difference in arrival for each waveform as compared to the first waveform is calculated; 3) plot of arrival time difference versus distance along the aorta, and the inverse of the linear regression line is the multiplane averaged PWV for the entire aorta. **(E)** Aortic flow visualization by streamlines in 4D flow MRI in a 67-year-old female without known aortic disease. Streamlines connect all the vector field points into a line and represent the instantaneous flow field within the aorta. Three different phases of peak systole, late systole, and diastole are shown and the velocity the streamline is represented by color (**red** is faster, **blue** is slower).

echocardiography, the maximum and minimum cross-sectional areas of the aorta at a region of interest are measured and the distensibility is calculated with the pulse pressure (Equation 2) (20). Benefits to this technique include the excellent spatial resolution of CT as well as the use of area measurements instead of simple diameters. One disadvantage is the decreased temporal resolution, which may lead to underestimation of distensibility if the time point at which maximal distention is not captured. The major drawback to this technique relates to the ionizing radiation exposure associated with CT imaging, as it requires continuous CT imaging during the entire cardiac cycle (20).

MAGNETIC RESONANCE IMAGING. MRI utilizes strong magnetic fields and nonionizing radiation to form images from the target molecules' response to radiowave energy input (44). By adjusting the input signal, various tissue properties can be highlighted and quantified and images formed (44). The measure of velocity can be quantified using PC techniques, which is based on blood flowing in a magnetic field resulting in a phase shift which is proportional to the velocity (45). By acquiring multiple velocity maps over the entire heart cycle, a cine can be produced showing the velocity changes over time and subsequently, with vessel area, the blood flow can be calculated (45). Similar to echocardiography, the measures of velocity and flow are applied to the blood traveling in the aorta and are useful in disease states such as coarctation (46) with the advantages of complete thorax coverage for collateral localization and extremely accurately flow quantification.

Using steady-state free precession cine imaging, MRI can also measure aortic distensibility by calculating the systolic and diastolic areas of any region of the aorta and applying Equation 2. Studies have also demonstrated the ability to substitute gradient echo PC imaging for steady-state free precession, which has the advantage of decreasing the imaging time if PWV from PC imaging is also being calculated (47).

Pulse wave velocity can be measured using 2D PC cine velocity or flow curves to calculate pulse wave arrival time at various locations within the aorta. **Central Illustration** panel C demonstrates a common application of calculating the aortic arch PWV (48) and compared with invasive pressure catheters, MRI has demonstrated good agreement (49). Due to the widespread availability of this MRI technique, several publications of age-stratified normals have been produced (50–53). Benefits of the 2D technique are widespread familiarity with 2D PC imaging, regional assessment capabilities, relatively short scan times, and good temporal resolution (10 to 20 ms).

Additional improvements to measuring PWV by MRI include the use of multiple planes, which improves the accuracy of calculating pulse wave velocity (54). With this technique, multiple points of analysis along the length of the aorta are utilized and linear regression is employed to determine PWV in the region of interest (see **Central Illustration**, panel D, as applied to 4-dimensional [4D] flow imaging). This technique has been further developed and enhanced with the addition of 2-directional in-plane velocity encoding which improves the accuracy of this measurement (55).

Recently, improvements in the acquisition of multidirectional PC imaging have led to significantly more research utilizing this technique to investigate aortic pathophysiology. 3D 3-directionally encoded cine velocity imaging (also known 3D cine PC or, used in this paper, 4D flow) acquires velocity information in all 3 directions at all locations within a defined volume. Utilizing post-processing software to calculate PWV, the velocity waveforms can be acquired post-imaging for any regional location and the technique of multiple plane and linear regression can be employed to diminish the impact of potential erroneous values (**Central Illustration**, panel D) (56,57). The acquisition time (5 to 15 min) and complexity of post-processing software has thus far limited the clinical utility of multiplanar techniques.

Four-dimensional flow technology also allows for unique visualization of the blood flow within the aorta. Several different techniques for visualizing this flow have been developed. These include vector fields, streamlines, and pathlines (58). Choice of visualization depends on the application of 4D flow, though often they are used in combination as the different techniques offer unique perspectives of blood flow in the aorta (**Central Illustration**, panel E).

With additional post-processing, 4D flow technology also provides the ability to calculate more complex hemodynamic measures including wall shear stress, flow displacement, helical flow, turbulence, and pressure gradients. Wall shear stress is the frictional force of blood on the endothelium and with the assistance of computational software, can be calculated from 4D flow datasets (59). Wall shear stress is implicated in vascular remodeling, endothelial dysfunction, and development of atherosclerosis (59–62). Flow displacement is a measure of how "off-center" the blood flow is from the center of the vessel lumen and semiquantifies abnormal flow within the aorta (26). Visualization and semiquantification of abnormal helical flow patterns has also been

developed using 4D flow and can discriminate those at risk for aneurysmal remodeling (63,64). Turbulence defined as nonlaminar and chaotic flow, is a contributing factor to aortic disease processes and its magnitude quantifiable by advanced post-processing calculations of 4D flow datasets (28). Turbulent kinetic energy, the energy within the areas of chaotic flow, has applications to post-stenotic flow and pressure gradients within the aorta (65). Pressure gradients are typically used to estimate the severity of an obstruction such as coarctation and can now be calculated using complex computational fluid dynamics (27).

APPLICATION TO AORTA IN DISEASE STATES

Flow and functional measurements can be applied to aortic diseases and be used in the investigation of pathologic mechanisms. Additionally, these measures may potentially aid in diagnoses, prognosis, and assessing disease severity (**Table 2**).

ARTERIOSCLEROSIS AND AGING. Defined as the thickening and stiffening of blood vessels, arteriosclerosis has been extensively studied with noninvasive imaging to determine its impact on function (24,53,54). Intertwined with vascular aging and hypertension, the changes associated with arteriosclerosis are described in **Figure 2**. For example, the PWV increases from approximately 7 m/s at 30 years of age and increases to 12 m/s at 70 years of age (24). This almost doubling of PWV implies an almost 4-fold change in the elastic modulus (Equation 3).

Previously thought to be simply a part of the normal aging process, abnormal arterial stiffening has been demonstrated as a predictor of adverse outcomes. Arterial stiffening leads to increased systolic and widened pulse pressures due to loss of both the ventricular contraction cushioning as well as loss of the reflective wave dampening (6). These compound effects on afterload are thought to contribute to left ventricular hypertrophy and ultimately, predispose one to left ventricular failure (66,67). Furthermore, it has been hypothesized that the loss of dampening also results in increased pulsations being transmitted to the vulnerable tissues such as the kidney and brain leading to microvascular and end-organ damage (68).

Using the Framingham cohort, cfPWV was demonstrated to be an independent risk factor for first CV event and improved risk prediction when added to the Framingham risk model (69). A recent meta-analysis of over 15,000 participants showed cfPWV to be an independent predictor of CV events and overall mortality in the general population (70). Furthermore, it was estimated that an increase of 1 m/s increased the risk of mortality increases 15% even after adjusting for known CV risk factors. The strength of findings like this has led to the recommendation by the European Society of Cardiology to include PWV assessment in the risk stratification of hypertensive individuals as a means of determining end-organ damage (71).

Similar predictive value of MRI-derived aortic distensibility for all-cause mortality was shown in a population free of known CV disease from the MESA (Multi-Ethnic Study of Atherosclerosis) study (72). In those with low and intermediate risk for CV disease, aortic distensibility also independently predicted CV events. In the Dallas Heart Study, elevated pulse wave velocity of the aortic arch by MRI was independently associated with nonfatal extra-cardiac vascular events with a modest improvement to the Framingham risk score (73).

TABLE 2 Aortic Diseases and Potential Applications of Hemodynamic Measurements of Potential Value

Disease	Noninvasive Imaging Assessment of Aortic Function or Flow	Potential Value
Arteriosclerosis/hypertension	• PWV • Distensibility	• Assess risk of cardiovascular event and overall mortality
Abdominal aneurysm	• Flow	• Visualize and quantify complications (e.g., endoleaks) post-endovascular repair
Chronic kidney disease	• PWV • Distensibility	• Assess risk of cardiovascular events and overall mortality
Vasculitis	• Strain • Distensibility • PWV	• Assess extent of detrimental hemodynamic effects of inflammation
Cancer therapy	• PWV • Distensibility	• Investigate as a mechanism for left ventricular dysfunction and increased CV events associated with cardiotoxic cancer therapy
Bicuspid aortic valve	• PWV • Distensibility • Flow pattern and flow displacement • Wall shear stress	• Assess risk of aortic root dilation
Hypertrophic cardiomyopathy	• PWV	• Investigate the association of aortic stiffness with increased myocardial fibrosis
Marfan syndrome	• Aortic wall strain • Distensibility of the aortic root • Regional PWV • Flow pattern	• Assess risk of aortic root dilation and dissection. • Quantify response to pharmacology therapy. • Post-operatively, visualize and quantify risk of adverse remodeling.
Coarctation of the aorta	• Pressure gradient • Aortic and collateral flow	• Assessment of the severity of stenosis and quantify collaterals. • Assess adequacy of stenosis correction and post-operatively, predict risk of restenosis or aneurysm formation

CV = cardiovascular; PWV = pulse wave velocity.

ATHEROSCLEROSIS. A distinct concept to arteriosclerosis but closely related by common, overlapping pathologic processes, atherosclerosis includes lipid deposition, inflammation, fibrosis, and calcification within the vessel wall (74). Though several studies have demonstrated aortic stiffness is associated with atherosclerotic risk factors such as hyperlipidemia, smoking, obesity, and diabetes mellitus, an interesting meta-analysis suggests that these associations are rather weak and that age and hypertension have the strongest degree of association with cfPWV (75). Similar to vascular aging, atherosclerosis adversely remodels the arterial wall leading to a loss of normal function. Atherosclerosis and calcification of the coronary arteries as well as the thoracic aorta was shown to be strongly associated with decreased gated CT-derived distensibility in the aorta (76). This was further demonstrated in longitudinal evaluation of aortic distensibility by gated CT and coronary artery atherosclerosis, which revealed parallel progression of coronary artery atherosclerosis and worsening aortic distensibility even after accounting for known risk factors including age (77).

Furthermore, cfPWV is independently associated with other noninvasive markers of atherosclerosis and end-organ damage including ankle-brachial index and the presence of brain white matter hyperintensity (78). Flow visualization has also been used to assess atherosclerotic disease. In a novel investigation utilizing 4D flow MRI, it was demonstrated that the descending aorta was a potential source for cryptogenic embolic stroke. Cine visualization of the particle trace lines within the descending aorta demonstrated retrograde aortic flow distal to the ostium of the left common carotid at the location of atheromatous plaques in the aorta (79).

ABDOMINAL ANEURYSM. Thought to be due to a complex interaction of genetic pre-disposition and exposure to atherosclerotic risk factors, abdominal aneurysms are defined by degradation of the elastic media and atheromatous changes in the intima (80). Using gated CT to link abnormal vessel mechanics to rupture, the aneurysmal portion of the abdominal aorta was found to be markedly less distensible than the more normal regions; however, there was no association between distensibility and aneurysm diameter, the traditional validated risk factor for aneurysm rupture (81). Additionally, 4D flow imaging has been demonstrated as a technique to visualize post-endovascular repair complications such as endoleaks, with the benefit of no intravenous contrast and quantification of direction and magnitude of the leak (82), though distortion artifacts particularly with stainless steel stents may limit the applicability of this technique.

BICUSPID AORTIC VALVE. The pathogenesis of the aortic abnormalities associated with bicuspid aortic valve as assessed by echo may be due to a primary aortopathy or a consequence of abnormal hemodynamics or a combination of the two (83). MRI reinforces these findings demonstrating that PWV in both the arch and descending aorta were increased in individuals with nonstenotic bicuspid valves and left ventricular mass and degree of regurgitant dysfunction were correlated to PWV (84).

In MRI, 4D flow has been used to help find potential hemodynamic markers that predispose individuals to root dilation and aneurysm formation. Jet direction and abnormal helical flow were 2 qualitative measures associated with bicuspid aortic valve (64). Other studies have demonstrated increased flow abnormalities associated with cusp-fusion subtype. These abnormal flow patterns lead to increased wall shear stress in those with bicuspid aortic valves (60–62). In a longitudinal study, flow displacement as measured by 4D flow sequences was found to be most correlated with growth of the aorta in bicuspid valve patients (85). A transesophageal echocardiography study of the descending aorta also demonstrated that in bicuspid aortic valve with severe aortic stenosis had altered distensibility as compared to those with tricuspid valve aortic stenosis, suggesting intrinsic alteration of aortic properties in bicuspids extending to the descending aorta (32).

CHRONIC KIDNEY DISEASE. CV disease is a major cause of morbidity and mortality in individuals with chronic kidney disease (CKD) and investigators have utilized measures of aortic function to further delineate this relationship (86–88). As assessed by MRI and echo, patients with early-stage CKD (86) as well as end-stage CKD (87) have reduced aortic distensibility. This increased aortic stiffness by means of cfPWV measurement has been shown to be an independent risk factor for all-cause mortality and CVD events in advanced CKD patients and improved risk prediction above traditional risk factors (88).

VASCULITIS. Kawasaki disease and Behcet's disease have been demonstrated to have detrimental effects on the function of the aorta, even in the absence of active aortic involvement of the disease (89–91). Using echo, individuals with Behcet's disease were demonstrated to have both reduced aortic strain and distensibility as compared to age-matched control subjects (89,90). In a cohort of Kawasaki disease, PWV in the aortic arch was elevated as assessed

by echo as compared to control subjects despite apparent resolution of the vasculitis (91).

TOXIN EXPOSURE. Anthracycline-based chemotherapy, used most frequently in breast cancer, lymphomas, and leukemias, has been associated with stiffening of the proximal portion of the aorta. Hypothesized to be due to oxidative stress, vascular matrix and endothelial dysfunction, aortic distensibility was adversely affected at 4 months post-anthracycline as compared to control subjects (92). A similar study demonstrated that the onset of adverse aortic stiffening was evident at 1 month after cancer treatment initiation and at 6 months. Furthermore, the aortic stiffening occurred concurrently with reductions in left ventricular ejection fraction and circumferential strain indicating potential aortoventricular interaction, which may have been responsible for the long-term cardiotoxic complications of cancer therapy including congestive heart failure (93).

HYPERTROPHIC CARDIOMYOPATHY. An inherited disorder associated with mutations in multiple genes encoding proteins of the cardiac sarcomere, abnormalities in aortic function have also been found. Aortic stiffness as assessed by MRI derived PWV in the arch was found to be elevated in individuals with hypertrophic cardiomyopathy. Additionally, those with extensive myocardial fibrosis tended to be even stiffer (94). Echo-derived aortic distensibility and vessel wall strain also have been shown to be reduced further supporting the notion that altered aortic elastic properties are present in patients with hypertrophic cardiomyopathy (95).

MARFAN SYNDROME. An autosomal dominant genetic disorder of the fibrillin protein that is present in the vascular wall, aortic pathology is common in Marfan syndrome patients (96). In a case-control study using MRI, the Marfan syndrome patients exhibited lower distensibility and increased PWV in the ascending aorta as compared to healthy subjects ($p < 0.01$). With beta-blocker therapy, the Marfan syndrome patients experienced a decrease in PWV and an improvement in ascending aortic distensibility and the control patients had no such changes (97). Furthermore, using MRI derived PWV in Marfan syndrome patients, the baseline aortic stiffness measurements were able to predict the absence of luminal dilation at 2 years of follow-up, offering another potential marker of risk stratification (98). Four-dimensional flow has shown potential for monitoring for complications post-valve sparing surgical replacement (99). Transesophageal echo also demonstrated that distensibility and tissue Doppler strain also could discriminate Marfan syndrome from normals and predict dilation and dissection (100).

COARCTATION OF THE AORTA. The congenital condition of narrowing at the ductus arteriosus was previously diagnosed with imaging using conventional angiography, but now MRI and echocardiography can both visualize the stenosis as well as assess the hemodynamic significance of the obstruction without the risks of ionizing radiation or nephrotoxic contrast agents. Using Doppler waveforms to measure the maximum velocity in the descending aorta, the peak pressure gradient at the stenosis was similar to cardiac catheterization (34).

MRI can demonstrate the existence of the narrowing and with PC imaging, assess both the pressure gradient across the coarctation and quantify the collateral flow within the thorax (46), and thereby select those in need of surgical repair. 4D flow imaging is also a proven method of quantification of collateral flow in patients with coarctation (101). With advanced post-processing techniques, 4D flow has also been demonstrated to accurately determine the peak-to-peak pressure gradients as compared to invasive catheterization (27). Additionally, noninvasive imaging can monitor post-operatively the adequacy of the correction as well as monitor serially for complications such as restenosis or aneurysm formation (46) or adverse remodeling of the aorta due to arch shape (102).

FUTURE INVESTIGATIONS. Future areas of research key to improving this multimodality approach to aortic disease include standardization of methodology in acquiring the measurements and creation of larger normative databases that have been normalized for age and sex. Subsequent development of normal and abnormal thresholds for each modality would allow for comparison across modalities and is key for integration into clinical practice.

Ongoing areas of research include the investigation of regional assessments of aortic stiffness and how certain disease processes may affect the proximal aorta, high in elastin content, as compared with the abdominal aorta, which has an increased propensity for atherosclerotic processes. Response to pharmacologic and nonpharmacologic interventions in various disease states is another important area of ongoing research that will aid with clinical decision making.

One area of rapidly expanding research is 4D flow imaging in MRI. With improvement in sequences, better post-processing software and validation of techniques, the applications to various aortic disease states are anticipated to grow rapidly. With these

improvements, larger longitudinal clinical trials are necessary to demonstrate the clinical utility of the novel hemodynamic measures and visualization capable with the technology. Another example of an innovative application of this technology is combining the cutting edge technologies of rapid prototyping with 3D printing and 4D flow MRI to construct hemodynamically accurate models of the aorta (103). With these models, patient-specific modeling and testing of procedural interventions and their impact on the aortic function are then possible.

CONCLUSIONS

The aorta is a complex structure, efficiently designed to transmit blood, buffer the vascular system from the pulsative ventricular contraction, and minimize reflective waves. The composition of the aorta is optimized to achieve these functions. In a complex interplay between changes in the composition of the aorta and pathologic hemodynamics, aging and disease cause perturbations in both the composition and hemodynamics. Noninvasive imaging techniques using echocardiography, cardiac CT, and MRI have been developed and can enable quantification of the changes in hemodynamics and improve diagnosis and risk prediction. Furthermore, these imaging techniques can assess the response of the aorta to both pharmacologic as well as surgical procedures and further predict prognosis or complications. With further development and research including longitudinal studies, noninvasive imaging assessment of aortic function and flow will likely become an integral part of the evaluation and diagnosis of aortic disease.

REPRINT REQUESTS AND CORRESPONDENCE: Dr. W. Gregory Hundley, Department of Internal Medicine, Section on Cardiovascular Medicine, Wake Forest School of Medicine, Medical Center Boulevard, Winston-Salem, North Carolina 27157. E-mail: ghundley@wakehealth.edu.

REFERENCES

1. Nichols WW. McDonald's Blood Flow in Arteries: Theoretical, Experimental and Clinical Principles. 6th edition. London, England: Hodder Arnold, 2011.

2. Westerhof N, Lankhaar J-W, Westerhof BE. The arterial Windkessel. Med Biol Eng Comput 2008; 47:131–41.

3. O'Rourke MF, Nichols WW. Aortic diameter, aortic stiffness, and wave reflection increase with age and isolated systolic. Hypertension 2005;45: 652–8.

4. Sunagawa K, Maughan WL, Burkhoff D, Sagawa K. Left ventricular interaction with arterial load studied in isolated canine ventricle. Am J Physiol 1983;245:H773–80.

5. De Tombe PP, Jones S, Burkhoff D, Hunter WC, Kass DA. Ventricular stroke work and efficiency both remain nearly optimal despite altered vascular loading. Am J Physiol 1993;264: H1817–24.

6. O'Rourke MF, Hashimoto J. Mechanical factors in arterial aging: a clinical perspective. J Am Coll Cardiol 2007;50:1–13.

7. Gasser TC, Ogden RW, Holzapfel GA. Hyperelastic modelling of arterial layers with distributed collagen fibre orientations. J R Soc Interface 2006;3:15–35.

8. Nijst P, Verbrugge FH, Grieten L, et al. The pathophysiological role of interstitial sodium in heart failure. J Am Coll Cardiol 2015;65:378–88.

9. Celermajer DS, Sorensen KE, Spiegelhalter DJ, Georgakopoulos D, Robinson J, Deanfield JE. Aging is associated with endothelial dysfunction in healthy men years before the age-related decline in women. J Am Coll Cardiol 1994;24:471–6.

10. Lakatta EG, Wang M, Najjar SS. Arterial aging and subclinical arterial disease are fundamentally intertwined at macroscopic and molecular levels. Med Clin North Am 2009;93:583–604.

11. Dingemans KP, Teeling P, Lagendijk Jaap H, Becker AE. Extracellular matrix of the human aortic media: An ultrastructural histochemical and immunohistochemical study of the adult aortic media. Anat Rec 2000;258:1–14.

12. Lee RT, Kamm RD. Vascular mechanics for the cardiologist. J Am Coll Cardiol 1994;23:1289–95.

13. Wolinsky H, Glagov S. A lamellar unit of aortic medial structure and function in mammals. Circ Res 1967;20:99–111.

14. Safar ME, Levy BI, Struijker-Boudier H. Current perspectives on arterial stiffness and pulse pressure in hypertension and cardiovascular diseases. Circulation 2003;107:2864–9.

15. Selvin E, Najjar SS, Cornish TC, Halushka MK. A comprehensive histopathological evaluation of vascular medial fibrosis: insights into the pathophysiology of arterial stiffening. Atherosclerosis 2010;208:69–74.

16. Spina M, Garbisa S, Hinnie J, Hunter JC, Serafini-Fracassini A. Age-related changes in composition and mechanical properties of the tunica media of the upper thoracic human aorta. Arterioscler Thromb Vasc Biol 1983;3:64–76.

17. Fleenor BS, Marshall KD, Durrant JR, Lesniewski LA, Seals DR. Arterial stiffening with ageing is associated with transforming growth factor-β1-related changes in adventitial collagen: reversal by aerobic exercise. J Physiol 2010;588: 3971–82.

18. Lorenz CH. The range of normal values of cardiovascular structures in infants, children, and adolescents measured by magnetic resonance imaging. Pediatr Cardiol 2000;21:37–46.

19. Virmani R, Avolio AP, Mergner WJ, et al. Effect of aging on aortic morphology in populations with high and low prevalence of hypertension and atherosclerosis. Comparison between occidental and Chinese communities. Am J Pathol 1991;139: 1119–29.

20. Ganten M, Boese JM, Leitermann D, Semmler W. Quantification of aortic elasticity: development and experimental validation of a method using computed tomography. Eur Radiol 2005;15:2506–12.

21. Laurent S, Cockcroft J, Bortel LV, et al. Expert consensus document on arterial stiffness: methodological issues and clinical applications. Eur Heart J 2006;27:2588–605.

22. McEniery CM, Cockcroft JR, Roman MJ, Franklin SS, Wilkinson IB. Central blood pressure: current evidence and clinical importance. Eur Heart J 2014;35:1719–25.

23. Bramwell JC, Hill AV. The velocity of the pulse wave in man. Proc R Soc Lond B Biol Sci 1922;93: 298–306.

24. Reference Values for Arterial Stiffness' Collaboration. Determinants of pulse wave velocity in healthy people and in the presence of cardiovascular risk factors: "establishing normal and reference values." Eur Heart J 2010;31:2338–50.

25. Sniecinski RM. Bernoulli: still simple, still useful. Anesth Analg 2014;119:1238–40.

26. Sigovan M, Hope MD, Dyverfeldt P, Saloner D. Comparison of four-dimensional flow parameters for quantification of flow eccentricity in the ascending aorta. J Magn Reson Imaging 2011;34: 1226–30.

27. Riesenkampff E, Fernandes JF, Meier S, et al. Pressure fields by flow-sensitive, 4D velocity-encoded CMR in patients with aortic coarctation. J Am Coll Cardiol Img 2014;7:920–6.

28. Dyverfeldt P, Sigfridsson A, Kvitting J-PE, Ebbers T. Quantification of intravoxel velocity standard deviation and turbulence intensity by generalizing phase-contrast MRI. Magn Reson Med 2006;56:850–8.

29. Tajik AJ, Seward JB, Hagler DJ, Mair DD, Lie JT. Two-dimensional real-time ultrasonic imaging of the heart and great vessels. Technique, image orientation, structure identification, and validation. Mayo Clin Proc 1978;53:271–303.

30. Quiñones MA, Otto CM, Stoddard M, Waggoner A, Zoghbi WA. Recommendations for quantification of Doppler echocardiography: A report from the Doppler quantification task force of the nomenclature and standards committee of the American Society of Echocardiography. J Am Soc Echocardiogr 2002;15:167–84.

31. Vitarelli A, Giordano M, Germanò G, et al. Assessment of ascending aorta wall stiffness in hypertensive patients by tissue Doppler imaging and strain Doppler echocardiography. Heart 2010;96:1469–74.

32. Petrini J, Yousry M, Rickenlund A, et al. The feasibility of velocity vector imaging by transesophageal echocardiography for assessment of elastic properties of the descending aorta in aortic valve disease. J Am Soc Echocardiogr 2010;23:985–92.

33. Cinthio M, Ahlgren ÅR, Bergkvist J, Jansson T, Persson HW, Lindström K. Longitudinal movements and resulting shear strain of the arterial wall. Am J Physiol Heart Circ Physiol 2006;291:H394–402.

34. Mendelsohn AM, Banerjee A, Donnelly LF, Schwartz DC. Is echocardiography or magnetic resonance imaging superior for precoarctation angioplasty evaluation? Cathet Cardiovasc Diagn 1997;42:26–30.

35. Stefanadis C, Stratos C, Boudoulas H, Kourouklis C, Toutouzas P. Distensibility of the ascending aorta: comparison of invasive and noninvasive techniques in healthy men and in men with coronary artery disease. Eur Heart J 1990;11:990–6.

36. Lim Y-H, Enkhdorj R, Kim BK, Kim SG, Kim JH, Shin J. Correlation between proximal abdominal aortic stiffness measured by ultrasound and brachial-ankle pulse wave velocity. Korean Circ J 2013;43:391–9.

37. Lang RM, Cholley BP, Korcarz C, Marcus RH, Shroff SG. Measurement of regional elastic properties of the human aorta. A new application of transesophageal echocardiography with automated border detection and calibrated subclavian pulse tracings. Circulation 1994;90:1875–82.

38. Go OD, Safar ME, Smulyan H. Assessment of aortic stiffness by transesophageal echocardiography. Echocardiography 2014;31:1105–12.

39. Drozdz J, Krzemińska-Pakuøla M, Lipiec P, et al. Regional aortic function is correlated with intima-media thickness-insights from three-dimensional echocardiography. J Am Soc Echocardiogr 2005;18:789–94.

40. Nemes A, Geleijnse ML, Soliman OII, Anwar AM, Vletter WB, ten Cate FJ. Real-time three-dimensional echocardiography for regional evaluation of aortic stiffness. Eur J Echocardiogr 2007;8:161–2.

41. Jiang B, Liu B, McNeill KL, Chowienczyk PJ. Measurement of pulse wave velocity using pulse wave Doppler ultrasound: comparison with arterial tonometry. Ultrasound Med Biol 2008;34:509–12.

42. Calabia J, Torguet P, Garcia M, et al. Doppler ultrasound in the measurement of pulse wave velocity: agreement with the Complior method. Cardiovasc Ultrasound 2011;9:13.

43. Mahesh M, Cody DD. Physics of cardiac imaging with multiple-row detector CT. RadioGraphics 2007;27:1495–509.

44. Ridgway JP. Cardiovascular magnetic resonance physics for clinicians: part I. J Cardiovasc Magn Reson 2010;12:71.

45. Firmin DN, Nayler GL, Klipstein RH, Underwood SR, Rees RS, Longmore DB. In vivo validation of MR velocity imaging. J Comput Assist Tomogr 1987;11:751–6.

46. Hom JJ, Ordovas K, Reddy GP. Velocity-encoded cine MR imaging in aortic coarctation: functional assessment of hemodynamic events. RadioGraphics 2008;28:407–16.

47. Herment A, Lefort M, Kachenoura N, et al. Automated estimation of aortic strain from steady-state free-precession and phase contrast MR images. Magn Reson Med 2011;65:986–93.

48. Mohiaddin RH, Firmin DN, Longmore DB. Age-related changes of human aortic flow wave velocity measured noninvasively by magnetic resonance imaging. J Appl Physiol 1993;74:492–7.

49. Grotenhuis HB, Westenberg JJM, Steendijk P, et al. Validation and reproducibility of aortic pulse wave velocity as assessed with velocity-encoded MRI. J Magn Reson Imaging 2009;30:521–6.

50. Voges I, Jerosch-Herold M, Hedderich J, et al. Normal values of aortic dimensions, distensibility, and pulse wave velocity in children and young adults: a cross-sectional study. J Cardiovasc Magn Reson 2012;14:77.

51. Redheuil A, Yu W-C, Wu CO, et al. Reduced ascending aortic strain and distensibility earliest manifestations of vascular aging in humans. Hypertension 2010;55:319–26.

52. Kim EK, Chang S-A, Jang SY, et al. Assessment of regional aortic stiffness with cardiac magnetic resonance imaging in a healthy Asian population. Int J Cardiovasc Imaging 2013;29:57–64.

53. Hickson SS, Butlin M, Graves M, et al. The relationship of age with regional aortic stiffness and diameter. J Am Coll Cardiol Img 2010;3:1247–55.

54. Rogers WJ, Hu Y-L, Coast D, et al. Age-associated changes in regional aortic pulse wave velocity. J Am Coll Cardiol 2001;38:1123–9.

55. Westenberg JJM, de Roos A, Grotenhuis HB, et al. Improved aortic pulse wave velocity assessment from multislice two-directional in-plane velocity-encoded magnetic resonance imaging. J Magn Reson Imaging 2010;32:1086–94.

56. Markl M, Wallis W, Brendecke S, Simon J, Frydrychowicz A, Harloff A. Estimation of global aortic pulse wave velocity by flow-sensitive 4D MRI. Magn Reson Med 2010;63:1575–82.

57. Dyverfeldt P, Ebbers T, Länne T. Pulse wave velocity with 4D flow MRI: Systematic differences and age-related regional vascular stiffness. Magn Reson Imaging 2014;32:1266–71.

58. Stankovic Z, Allen BD, Garcia J, Jarvis KB, Markl M. 4D flow imaging with MRI. Cardiovasc Diagn Ther 2014;4:173–92.

59. Stalder AF, Russe MF, Frydrychowicz A, Bock J, Hennig J, Markl M. Quantitative 2D and 3D phase contrast MRI: Optimized analysis of blood flow and vessel wall parameters. Magn Reson Med 2008;60:1218–31.

60. Bissell MM, Hess AT, Biasiolli L, et al. Aortic dilation in bicuspid aortic valve disease: flow pattern is a major contributor and differs with valve fusion type. Circ Cardiovasc Imaging 2013;6:499–507.

61. Barker AJ, Markl M, Bürk J, et al. Bicuspid aortic valve is associated with altered wall shear stress in the ascending aorta. Circ Cardiovasc Imaging 2012;5:457–66.

62. Hope MD, Hope TA, Crook SES, et al. 4D flow CMR in assessment of valve-related ascending aortic disease. J Am Coll Cardiol Img 2011;4:781–7.

63. Kilner PJ, Yang GZ, Mohiaddin RH, Firmin DN, Longmore DB. Helical and retrograde secondary flow patterns in the aortic arch studied by three-directional magnetic resonance velocity mapping. Circulation 1993;88:2235–47.

64. Hope MD, Hope TA, Meadows AK, et al. Bicuspid aortic valve: four-dimensional MR evaluation of ascending aortic systolic flow patterns. Radiology 2010;255:53–61.

65. Dyverfeldt P, Hope MD, Tseng EE, Saloner D. Magnetic resonance measurement of turbulent kinetic energy for the estimation of irreversible pressure loss in aortic stenosis. J Am Coll Cardiol Img 2013;6:64–71.

66. Levy D, Larson MG, Vasan RS, Kannel WB, Ho KK. The progression from hypertension to congestive heart failure. JAMA 1996;275:1557–62.

67. Katz AM. Cardiomyopathy of overload. N Engl J Med 1990;322:100–10.

68. O'Rourke MF, Safar ME. Relationship between aortic stiffening and microvascular disease in brain and kidney: cause and logic of therapy. Hypertension 2005;46:200–4.

69. Mitchell GF, Hwang S-J, Vasan RS, et al. Arterial stiffness and cardiovascular events: The Framingham Heart Study. Circulation 2010;121:505–11.

70. Vlachopoulos C, Aznaouridis K, Stefanadis C. Prediction of cardiovascular events and all-cause mortality with arterial stiffness. J Am Coll Cardiol 2010;55:1318–27.

71. Members AF, Mancia G, Fagard R, et al. 2013 ESH/ESC Guidelines for the management of arterial hypertension. Eur Heart J 2013;34:2159–219.

72. Redheuil A, Wu CO, Kachenoura N, et al. Proximal aortic distensibility is an independent predictor of all-cause mortality and incident CV

events: the MESA study. J Am Coll Cardiol 2014;64:2619–29.

73. Maroules CD, Khera A, Ayers C, et al. Cardiovascular outcome associations among cardiovascular magnetic resonance measures of arterial stiffness: the Dallas heart study. J Cardiovasc Magn Reson 2014;16:33.

74. Tunick PA, Kronzon I. Atheromas of the thoracic aorta: clinical and therapeutic update. J Am Coll Cardiol 2000;35:545–54.

75. Cecelja M, Chowienczyk P. Dissociation of aortic pulse wave velocity with risk factors for cardiovascular disease other than hypertension a systematic review. Hypertension 2009;54:1328–36.

76. Siegel E, Thai W-E, Techasith T, et al. Aortic distensibility and its relationship to coronary and thoracic atherosclerosis plaque and morphology by MDCT: Insights from the ROMICAT Trial. Int J Cardiol 2013;167:1616–21.

77. Oberoi S, Schoepf UJ, Meyer M, et al. Progression of arterial stiffness and coronary atherosclerosis: longitudinal evaluation by cardiac CT. Am J Roentgenol 2013;200:798–804.

78. Coutinho T, Turner ST, Kullo IJ. Aortic pulse wave velocity is associated with measures of subclinical target organ damage. J Am Coll Cardiol Img 2011;4:754–61.

79. Harloff A, Strecker C, Frydrychowicz AP, et al. Plaques in the descending aorta: A new risk factor for stroke? Visualization of potential embolization pathways by 4D MRI. J Magn Reson Imaging 2007;26:1651–5.

80. Sakalihasan N, Limet R, Defawe O. Abdominal aortic aneurysm. The Lancet 2005;365:1577–89.

81. Ganten M-K, Krautter U, von Tengg-Kobligk H, et al. Quantification of aortic distensibility in abdominal aortic aneurysm using ECG-gated multi-detector computed tomography. Eur Radiol 2008;18:966–73.

82. Hope TA, Zarins CK, Herfkens RJ. Initial experience characterizing a type I endoleak from velocity profiles using time-resolved three-dimensional phase-contrast MRI. J Vasc Surg 2009;49:1580–4.

83. Nistri S, Sorbo MD, Basso C, Thiene G. Bicuspid aortic valve: abnormal aortic elastic properties. J Heart Valve Dis 2002;11:369–73; discussion 373–4.

84. Grotenhuis HB, Ottenkamp J, Westenberg JJM, Bax JJ, Kroft LJM, de Roos A. Reduced aortic elasticity and dilatation are associated with aortic regurgitation and left ventricular hypertrophy in nonstenotic bicuspid aortic valve patients. J Am Coll Cardiol 2007;49:1660–5.

85. Hope MD, Sigovan M, Wrenn SJ, Saloner D, Dyverfeldt P. MRI hemodynamic markers of progressive bicuspid aortic valve-related aortic disease. J Magn Reson Imaging 2014;40:140–5.

86. Edwards NC, Ferro CJ, Townend JN, Steeds RP. Aortic distensibility and arterial-ventricular coupling in early chronic kidney disease: a pattern resembling heart failure with preserved ejection fraction. Heart 2008;94:1038–43.

87. Doyle A, Mark PB, Johnston N, et al. Aortic stiffness and diastolic flow abnormalities in end-stage renal disease assessed by magnetic resonance imaging. Nephron Clin Pract 2008;109:c1–8.

88. Karras A, Haymann J-P, Bozec E, et al. Large artery stiffening and remodeling are independently associated with all-cause mortality and cardiovascular events in chronic kidney disease. Hypertension 2012;60:1451–7.

89. Ikonomidis I, Lekakis J, Stamatelopoulos K, Markomihelakis N, Kaklamanis PG, Mavrikakis M. Aortic elastic properties and left ventricular diastolic function in patients with Adamantiades-Behcet's disease. J Am Coll Cardiol 2004;43:1075–81.

90. Tunc SE, Dogan A, Gedikli O, Arslan C, Sahin M. Assessment of aortic stiffness and ventricular diastolic functions in patients with Behçet's disease. Rheumatol Int 2005;25:447–51.

91. Vaujois L, Dallaire F, Maurice RL, et al. The biophysical properties of the aorta are altered following Kawasaki disease. J Am Soc Echocardiogr 2013;26:1388–96.

92. Grover S, Lou PW, Bradbrook C, et al. Early and late changes in markers of aortic stiffness with breast cancer therapy. Intern Med J 2014:140–7.

93. Drafts BC, Twomley KM, D'Agostino R Jr., et al. Low to moderate dose anthracycline-based chemotherapy is associated with early noninvasive imaging evidence of subclinical cardiovascular disease. J Am Coll Cardiol Img 2013;6:877–85.

94. Boonyasirinant T, Rajiah P, Setser RM, et al. Aortic stiffness is increased in hypertrophic cardiomyopathy with myocardial fibrosis. J Am Coll Cardiol 2009;54:255–62.

95. Gavallér H, Sepp R, Csanády M, Forster T, Nemes A. Hypertrophic cardiomyopathy is associated with abnormal echocardiographic aortic elastic properties and arteriograph-derived pulse-wave velocity. Echocardiography 2011;28:848–52.

96. Ho NC, Tran JR, Bektas A. Marfan's syndrome. The Lancet 2005;366:1978–81.

97. Groenink M, de Roos A, Mulder BJ, Spaan JA, van der Wall EE. Changes in aortic distensibility and pulse wave velocity assessed with magnetic resonance imaging following beta-blocker therapy in the Marfan syndrome. Am J Cardiol 1998;82:203–8.

98. Kröner ESJ, Scholte AJHA, de Koning PJH, et al. MRI-assessed regional pulse wave velocity for predicting absence of regional aorta luminal growth in marfan syndrome. Int J Cardiol 2013;167:2977–82.

99. Kvitting J-PE, Ebbers T, Wigström L, Engvall J, Olin CL, Bolger AF. Flow patterns in the aortic root and the aorta studied with time-resolved, 3-dimensional, phase-contrast magnetic resonance imaging: implications for aortic valve-sparing surgery. J Thorac Cardiovasc Surg 2004;127:1602–7.

100. Vitarelli A, Conde Y, Cimino E, et al. Aortic wall mechanics in the marfan syndrome assessed by transesophageal tissue doppler echocardiography. Am J Cardiol 2006;97:571–7.

101. Hope MD, Meadows AK, Hope TA, et al. Clinical evaluation of aortic coarctation with 4D flow MR imaging. J Magn Reson Imaging 2010;31:711–8.

102. Ou P, Celermajer DS, Raisky O, et al. Angular (Gothic) aortic arch leads to enhanced systolic wave reflection, central aortic stiffness, and increased left ventricular mass late after aortic coarctation repair: Evaluation with magnetic resonance flow mapping. J Thorac Cardiovasc Surg 2008;135:62–8.

103. Canstein C, Cachot P, Faust A, et al. 3D MR flow analysis in realistic rapid-prototyping model systems of the thoracic aorta: Comparison with in vivo data and computational fluid dynamics in identical vessel geometries. Magn Reson Med 2008;59:535–46.

KEY WORDS aorta, aorta hemodynamics, aortic disease, distensibility, pulse wave velocity